



Determination of onset temperature of melting in binary alloys using unit root test in differential scanning calorimetry

Jiwon Park¹ · Kil-Won Moon² · Chang-Seok Oh¹ · Joo-Hee Kang¹ · Jeki Jung^{1,3} · Youho Lee⁴ · Dongju Kim⁴

Received: 7 April 2023 / Accepted: 18 September 2023 / Published online: 10 October 2023
© Akadémiai Kiadó, Budapest, Hungary 2023

Abstract

One of the important functions in differential scanning calorimetry (DSC) measurements is to determine the phase transition temperature of materials. In this study, we propose a statistical approach to determine the onset temperature of melting in multiphase alloys using the heating curve of DSC. The melting temperature determined using the extrapolation method is noticeably different from the detectable onset temperature of the reaction. The stationarity of the baseline (of the DSC curve) enables the detection of the onset temperature using statistical method without assumptions of shape of the heat absorption peak; the onset temperature of melting is the point where the baseline loses stationarity which was determined in augmented Dickey-Fuller test in this study. The method was validated by melting a potential eutectic reference alloy (Ag–40Cu in atomic percent), which has an invariant melting temperature at the eutectic composition. The onset temperatures of eutectic and congruent melting of a few binary alloys (Co–13Nb, Ni–41Nb, Ni–45Pd) were determined using this method and compared with the melting temperature obtained using the extrapolation method. The present study provides an improved methodology to evaluate the accurate phase transition temperature of a material.

Keywords DSC · Alloy · Augmented Dickey-Fuller test · Onset temperature of melting

Introduction

Since the physical and mechanical properties of a material depend on its phase, correct knowledge of the phase transition temperature is important in multiple applications. Differential scanning calorimetry (DSC) is a powerful method for exploring the thermal properties and phase transition behaviors of materials. By monitoring the heat flow difference between the specimen and a reference, the phase transitions accompanying enthalpy changes, such as melting and solidification of metals, can be easily observed. ASTM

E794 [1] and E967–18 [2] define the standard test method for determining the melting and crystallization temperatures of materials using DSC. They employ the extrapolation method to determine the onset temperature of phase transition, which is also commonly used to determine the melting (solidus) temperature [3]. However, a discrepancy exists between the temperature evaluated using the extrapolation method and the detectable onset temperature from the baseline of DSC curve during the melting of the alloy, even in invariant reactions [4]. The intersection of the baseline and a tangent to the peak also depends on peak shape. The sharpness of the transition from baseline to peak and peak linearity depend on the sensitivity of sensor. Meanwhile, homogeneity of sample affects the peak singularity. Selecting the detectable departure temperature from the baseline as the onset temperature of phase transition is further limited by the noise of the acquired signal. To address these problems, trend determination techniques and the concept of stationarity from time series analysis were adopted in this work. A stationary time series with white noise exhibits constant mean and variance [5]. The discrimination of non-stationarity of time series is by detecting departures of the statistical properties of the time series. Analogous departure

✉ Jiwon Park
jiwonp@kims.re.kr

¹ Korea Institute of Materials Science, 797 Changwondaero, Changwon 51508, Republic of Korea

² National Institute of Standards and Technology, 100 Bureau Drive, Gaithersburg, MD 20899, USA

³ Department of Materials Science and Engineering, Pusan National University, 2 Busandaehakro 63Beongil, Busan 46241, Republic of Korea

⁴ Department of Nuclear Engineering, Seoul National University, 1 Gwanakro, Seoul 08826, Republic of Korea

from the baseline can then be assessed from the statistics of the DSC data. The temperature versus heat evolution may substitute time versus heat evolution because the heating (cooling) rate is generally constant during DSC analysis, depending on heat capacity without phase transition under a constant heating rate. This implies that the detectable departure temperature from the baseline can be determined statistically using stationarity determination techniques of time series, such as a unit root test [6]. Moreover, this method is devoid of the limitations of the extrapolation method which arise from peak linearity and singularity.

This study aims to propose a robust method of detecting the onset temperature of phase transition using signal departure from the baseline in a statistical approach. The onset temperature of phase transition is the point where the baseline loses stationarity, which is determined in a unit root test. The peak geometry does not influence the onset temperature solely determined from the baseline.

Method and materials

Unit root test

The stationarity or trend stationarity of stochastic processes can be determined using a unit root test. A schematic comparison of stationarity, trend stationarity, and non-stationarity is illustrated in Fig. 1. When the characteristic equation of an autoregressive process described in Eq. (1) has a unit root, the process is nonstationary.

$$y_t = \rho_1 y_{t-1} + \rho_2 y_{t-2} + \dots + \rho_k y_{t-k} + \varepsilon_t \quad (1)$$

In Eq. (1), y_t is the observed value at time t , k is the order of process, and ε_t is white noise (i.e., independent and normally distributed with mean zero and variance σ^2). The characteristic equation of (1) with multiplicity one is:

$$r^k - r^{k-1}\rho_1 - r^{k-2}\rho_2 - \dots - \rho_k = 0 \quad (2)$$

When $r = 1$ is a root of Eq. (2), the Eq. (1) has a unit root, which implies that y_t depends on y_{t-1} , y_{t-2} , and eventually y_0 . In a unit root test, the null hypothesis is that the process having a unit root is nonstationary, and the alternative hypothesis is that it is stationary. The augmented Dickey-Fuller

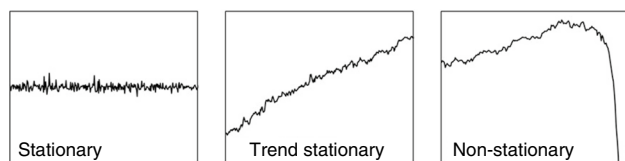


Fig. 1 Schematic comparison between stationarity, trend-stationarity, and non-stationarity

(ADF) test [6] is one of the most popular unit root tests and is easily accessible through Python [7] modules, such as the *statsmodels* package [8]. In this study, the ADF test was used to determine the stationarity of the process when the first difference of the acquired signal (h_t) is set y_t in Eq. (3). In the DSC analysis, temperature is equivalent to time because the heating rate during measurement is fixed.

$$y_t = h_t - h_{t-1} \quad (3)$$

Materials and analyses

A potential reference metal and three binary alloys were used to analyze the calorimetric behavior near the four invariant melting temperatures (eutectic and congruent melting). The materials used in this study and the relevant reactions are listed in Table 1. Binary alloy ingots near eutectic compositions were prepared via vacuum arc melting with reagent-grade materials where the purities of starting elements are equal or better than 99.9%. The specimens were cut from the as-cast ingots and tested using a Netzsch DSC404F1¹ with an alumina pan and lid under 6N argon atmosphere. DSC measurements were conducted for cyclic heating and cooling between 100 °C above and 300 °C below the melting temperature five times for different heating rates, except for the Ag-40Cu alloys that cycled twice or five times (Supplementary material). The data with the heating rate of 10 °C min⁻¹ and the cooling rate of 40 °C min⁻¹ are used to determine the onset temperature with the unit root test. The post-DSC microstructures were analyzed by scanning electron microscopy (SEM) using a JEOL JSM-7900F instruments. The specimens were ground and polished with diamond and colloidal silica suspensions without chemical etching to minimize topological interference in backscattered electron (BSE) observations.

Results and discussion

ADF test

Figure 2 shows the autocorrelation analysis of the baseline and the first difference of it in the DSC curve of Co-13Nb. The baseline in Fig. 2b, which depends on the heat capacity of the specimen and the measuring temperature, exhibits a positive slope with temperature. The stationarity of the process can be analyzed using the autocorrelation function

¹ Commercial names for instruments and software are used for completeness and do not constitute and endorsement from NIST.

Table 1 List of alloys and reactions

Alloy	Reaction type	Phases	Melting temperature /°C
Ag-40Cu*	Eutectic melting	FCC1 + FCC2 → Liquid	779 [9]
Ni-41Nb	Eutectic melting	Ni ₃ Nb + μ-Phase → Liquid	1175 [10]
Co-13Nb	Eutectic melting	FCC + Laves → Liquid	1239 [11]
Ni-45Pd	Congruent melting	FCC → liquid	1237 [12]

Asterisk (*) remarks on the potential reference material for temperature calibration. Compositional numbers are in atomic percent (at. %)

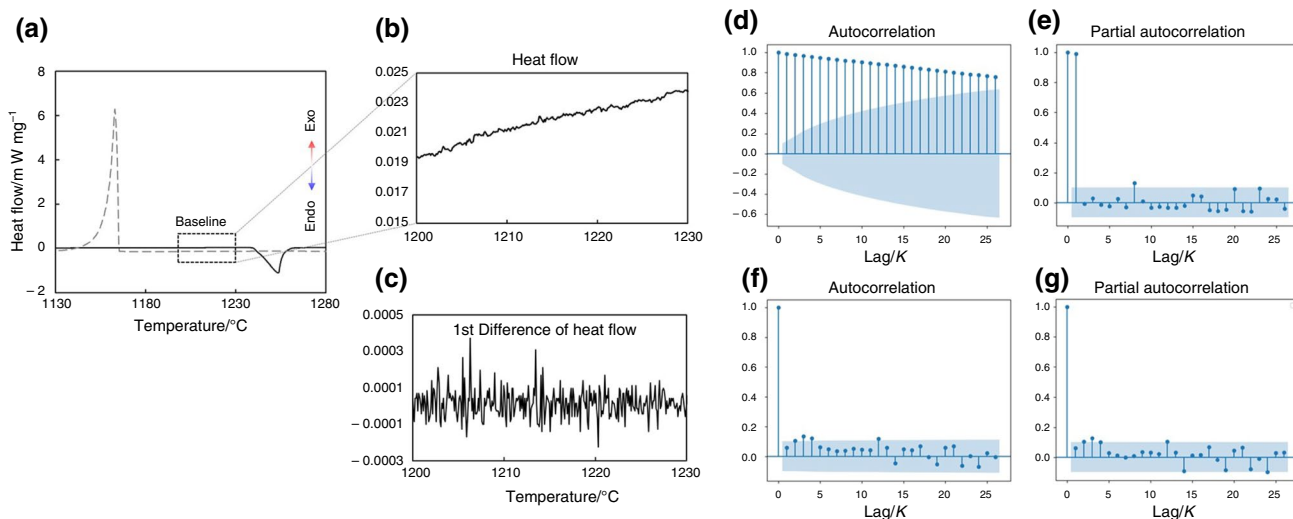


Fig. 2 Autocorrelation analysis of the baseline near melting temperature. **a** DSC curves of Co-13Nb. **b** Enlarged view of the baseline highlighted in (a). **c** First difference of the baseline shown in (b). **d**

ACF of (b). **e** PACF of (b). **f** ACF of (c). **g** PACF of (c). The shaded regions in (d-g) represent the confidence intervals

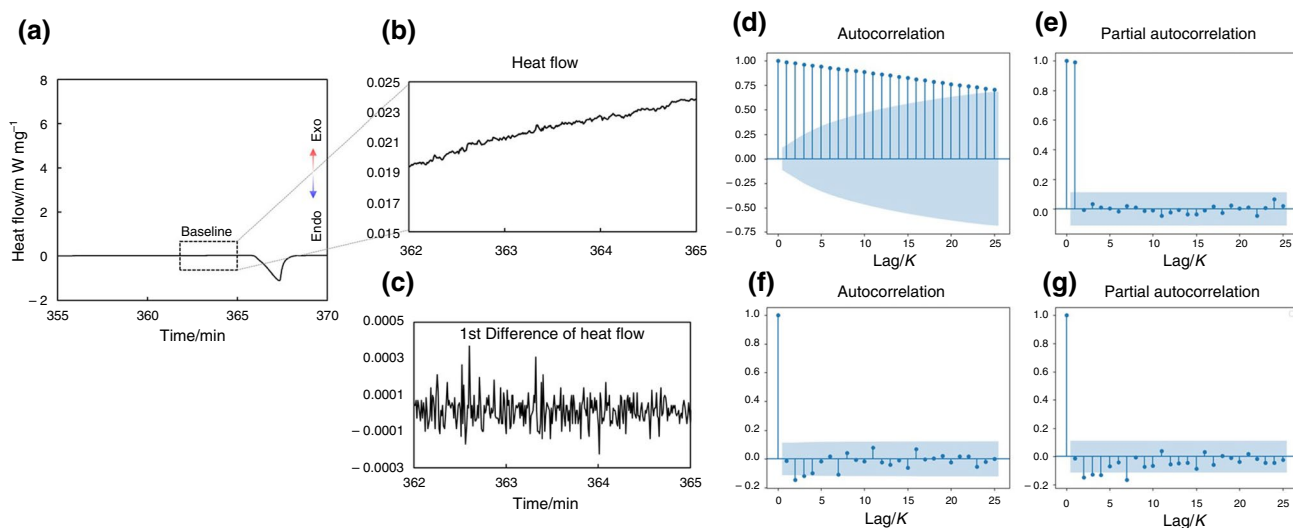


Fig. 3 Autocorrelation analysis of time vs. heat flow curve. **a** DSC curves of Co-13Nb with time. **b** Enlarged view of the baseline highlighted in (a). **c** First difference of the baseline shown in (b). **d**

ACF of (b). **e** PACF of (b). **f** ACF of (c). **g** PACF of (c). The shaded regions in (d-g) represent the confidence intervals

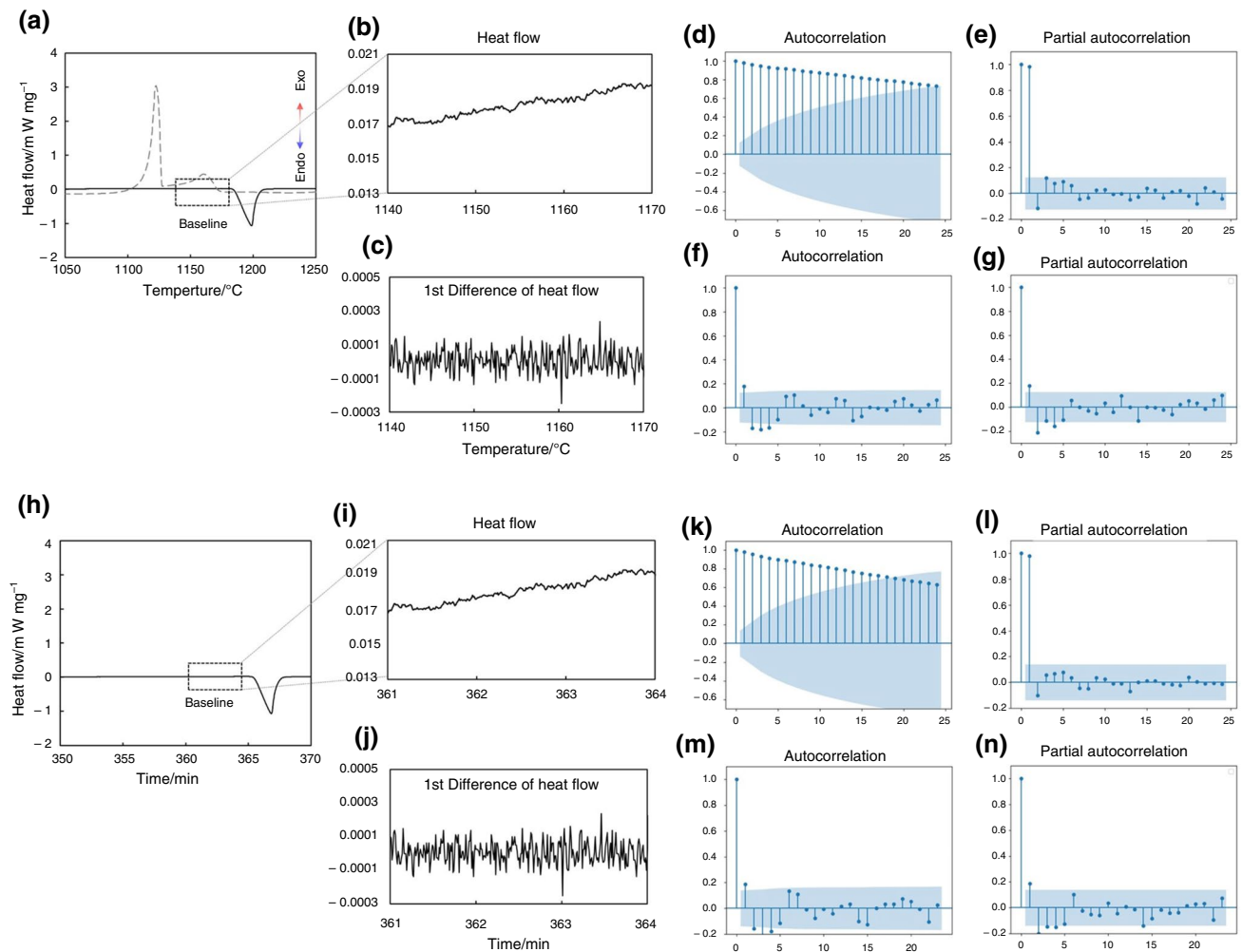


Fig. 4 Autocorrelation analysis of time vs. heat flow curve. **a** DSC curves of Ni-41Nb with temperature. **b** Enlarged view of the baseline highlighted in (a). **c** First difference of the baseline shown in (b). **d** ACF of (b). **e** PACF of (b). **f** ACF of (c). **g** PACF of (c). **h** DSC

curves of Ni-41Nb with time. **i** Enlarged view of the baseline highlighted in (i). **j** First difference of the baseline shown in (i). **k** ACF of (i). **l** PACF of (i). **m** ACF of (j). **n** PACF of (j). The shaded regions in (d–g) and (k–n) represent the confidence intervals

(ACF) and partial-autocorrelation function (PACF) with lag time (k) and are defined in Eqs. (4) and (5), respectively:

$$\text{ACF}(k) = \frac{\sum_{t=1}^{N-k} (y_t - \bar{y})(y_{t+k} - \bar{y})}{\sum_{t=1}^N (y_t - \bar{y})^2} \quad (4)$$

$$\text{PACF}(k) = \text{Corr}(y_t - \rho_t y_{t-1}, y_{t-k} - \rho_{t-k} y_{t-k-1}) = \text{Corr}(\varepsilon_t, \varepsilon_{t-k}) \quad (5)$$

ACF(k) represents the correlation of y at times t and $t-k$, and it rapidly decreases when the process is stationary. PACF(k) provides the correlation between y_t and y_{t-k} without the effects of $y_{t-1}, y_{t-2}, \dots, y_{t-k+1}$. The values of PACF decrease after $k=2$ when the process is stationary. The ACF and PACF of the baseline shown in Fig. 2d and e, respectively, exhibit slow convergence with the lag time.

In contrast, the ACF (Fig. 2f) and PACF (Fig. 2g) of the first difference of the baseline sharply decreased immediately after $k > 1$, indicating that the first differentiation of the DSC signal effectively removes the trend (positive slope) of the process. The identical analysis was performed for time versus heat flow curve to confirm the validity of method in Fig. 3. Similarly, the analyses on Ni-41Nb and Ni-45Pd curves are shown in Fig. 4 and Fig. 5, respectively.

The ADF test rejects the null hypothesis when the test statistic is less than the critical value [5], i.e., the process is stationary and set at the 95% significance level (p -value=0.05). The onset temperature of the phase transition can be obtained by monitoring the stationarity of the process using the ADF test in the moving-window approach with constant number of measured points, as shown in Fig. 6. Once the acquired DSC signal departs from the baseline in a

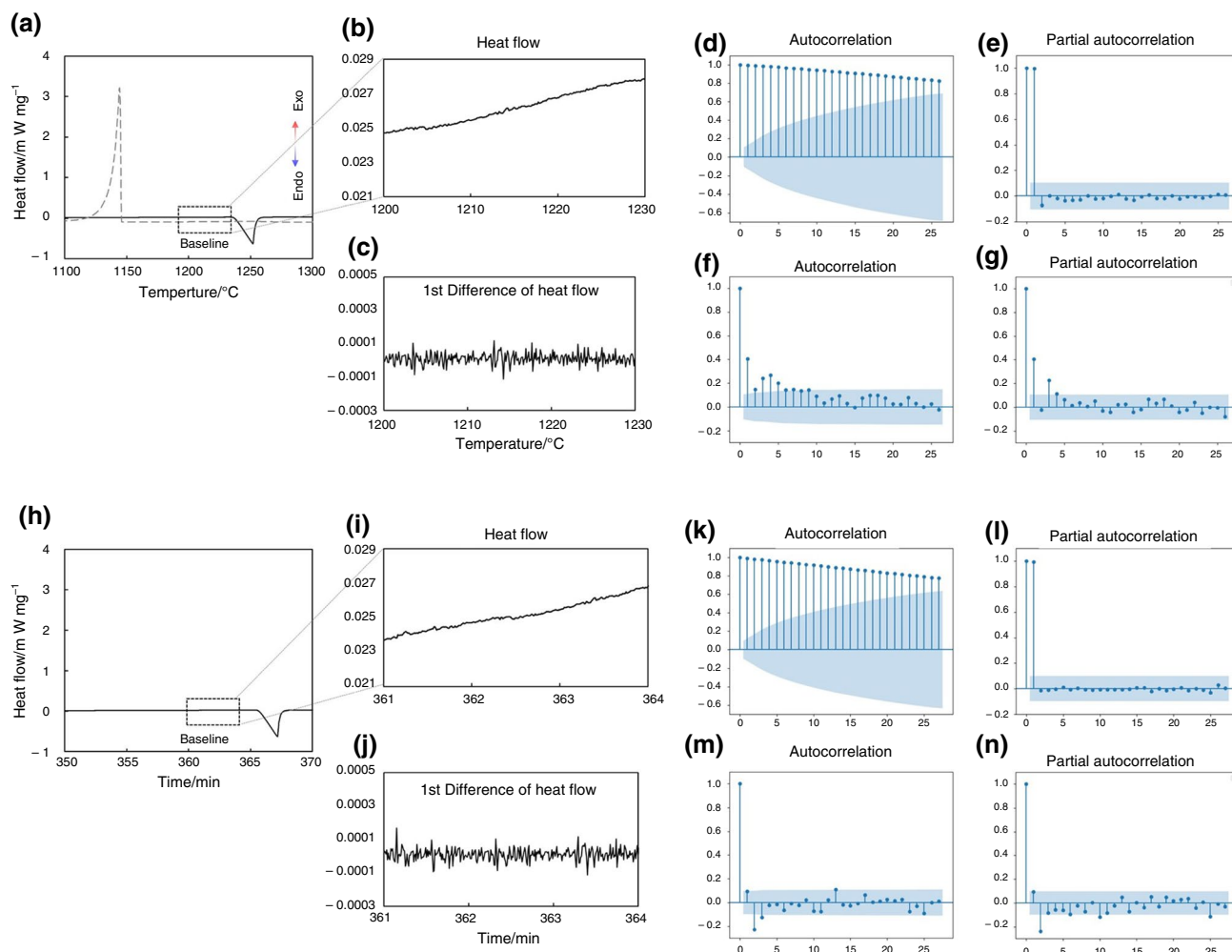


Fig. 5 Autocorrelation analysis of time vs. heat flow curve. **a** DSC curves of Ni-45Pd with temperature. **b** Enlarged view of the baseline highlighted in (a). **c** First difference of the baseline shown in (b). **d** ACF of (b). **e** PACF of (b). **f** ACF of (c). **g** PACF of (c). **h** DSC

curves of Ni-45Pd with time. **i** Enlarged view of the baseline highlighted in (i). **j** First difference of the baseline shown in (i). **k** ACF of (i). **l** PACF of (i). **m** ACF of (j). **n** PACF of (j). The shaded regions in (d-g) and (k-n) represent the confidence intervals

specific window, its first difference loses stationarity; therefore, the computed p-value becomes greater than 0.05. The onset temperature was determined from the highest temperature of the window during heating. The example in Fig. 6b shows that the ADF test result on the DSC curve gives only two values that are close to either zero or one. The abrupt jump in the p-value at the onset temperature indicates that the ADF test is robust.

Validation: eutectic melting of Ag-40Cu alloy

The above approach was validated using Ag-40Cu. Although eutectic melting of Ag-40Cu at 779 °C [9] is a commonly used invariant reaction for temperature calibration, it is often affected by reaction kinetics and instrumental error. Figure 7 shows the shift in the onset temperature

(T_{onset}) with different heating/cooling cycles acquired from independent specimens with identical measuring conditions (except for the number of cycles). Note that the specimens were cut from adjacent portion of the same ingot. The DSC curves show noticeable shift and disagreement between T_{onset} and the phase transition temperature determined by the extrapolation method (T_{extrap}). As shown in Figs. 7b and c, the representability of T_{extrap} determined by the extrapolation method strongly depends on the sharpness of the reaction signal at the position marked in Fig. 7a.

In order to compute p-values, an initial window between 760 and 775 °C, covering 150 measured points was set. The window was then progressively moved toward a higher temperature, and changes in the p-value was monitored. The p-values of the points marked with triangles in Figs. 7b and c were greater than 0.05. This suggests that, at those points, the first differences of the signal lost stationarity, and the

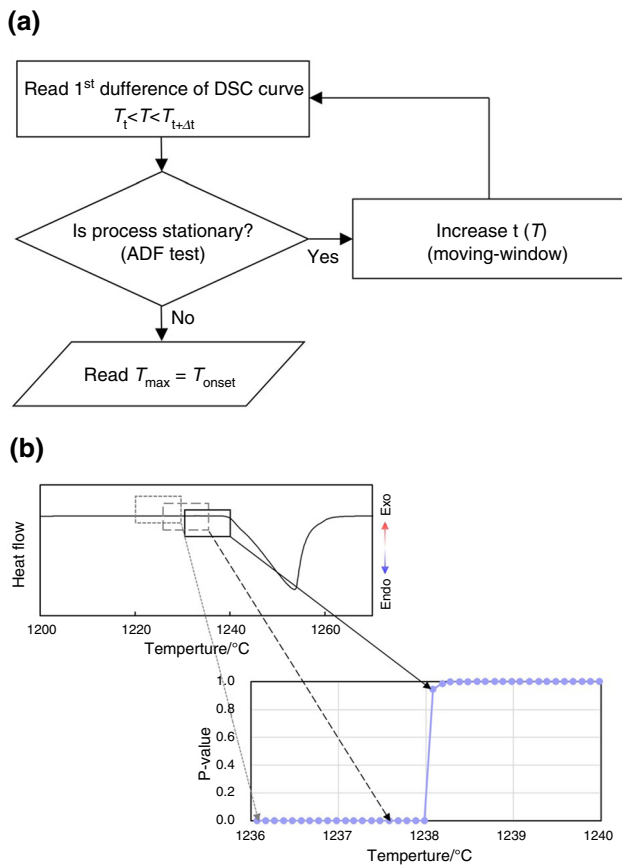


Fig. 6 **a** Flowchart of computing ADF statistics in moving window approach **b** schematic representation of moving window and p-value change in eutectic melting of Co-13Nb

signals departed from the baselines. This implies that it can also be used to determine the onset temperature of phase transition and, additionally, is independent of the shape of DSC curve.

Applications in eutectic / congruent melting and solidification

Co-13Nb alloy melted from a regular eutectic lamellar structure consisting of FCC and Laves phases near 1240 °C. As shown in Fig. 8, T_{onset} determined by the ADF test was 1238.1 °C, and T_{extrap} determined by the extrapolation method was 1239.7 °C. The observed microstructure is uniform lamellae eutectic. In contrast, the microstructure of the Ni-41Nb alloy near the eutectic composition exhibited a complex mixture of phases consisting of a faceted μ -phase, small dendritic Ni_3Nb , and an irregular eutectic structure (Fig. 9). T_{onset} and T_{extrap} measured from this alloy were, 1176.2 and 1178.2 °C, respectively, implying inhomogeneous melting. Congruent melting of Ni-45Pd alloy in Fig. 10 shows the most significant difference between T_{onset} and T_{extrap} , which are 1234.5 and 1237.1 °C, respectively.

The determination of T_{extrap} requires two linear fits from the baseline and the heat absorption peak [2, 3]. Therefore, the peak singularity significantly influences the value of T_{extrap} : when the peak exhibits inflection points, T_{extrap} varies with the choice of the linear portion for the fitting. The heat absorption peaks and their slope changes are shown in Fig. 11. Two inflection points (marked with dashed lines) were observed in the heat absorption curve of Co-13Nb alloy, which lead to an inaccurate extrapolation. The T_{onset} determined by the ADF test is devoid of this problem because it solely depends on the baseline statistics without any interference from the peak shape.

Solidification of the alloys with invariant reactions exhibits a significant supercooling associated with the nucleation of solid from the melt, as shown in Fig. 8a, Fig. 9a, and Fig. 10a. Unlike the melting, the solidification temperature in each cycle substantially differs (Supplementary material). For that reason, the fifth cooling curves of the alloys associated with the observed microstructures are used for the analyses in Fig. 12. The

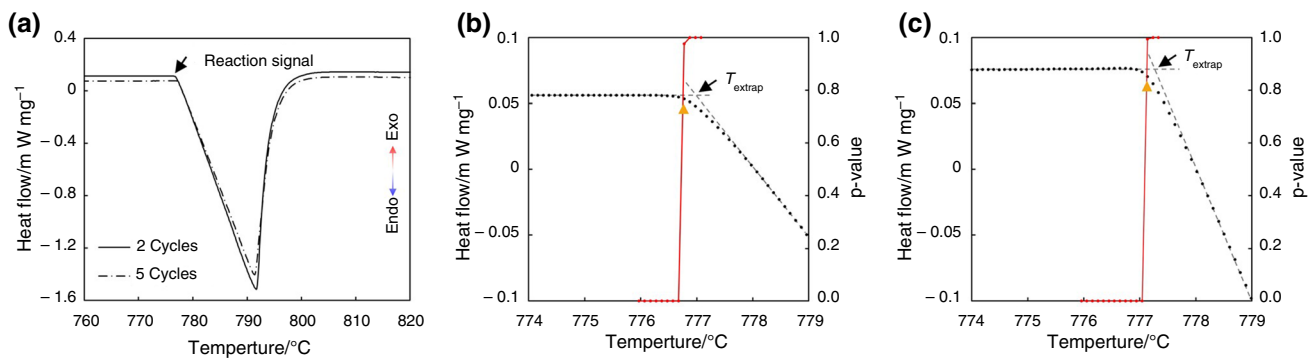


Fig. 7 **a** DSC plots of Ag-40Cu alloy with different numbers of heating/cooling cycles. DSC signals, p-values in each temperature, and the extrapolated temperatures in **b** 2-cycles and **c** 5-cycles specimens

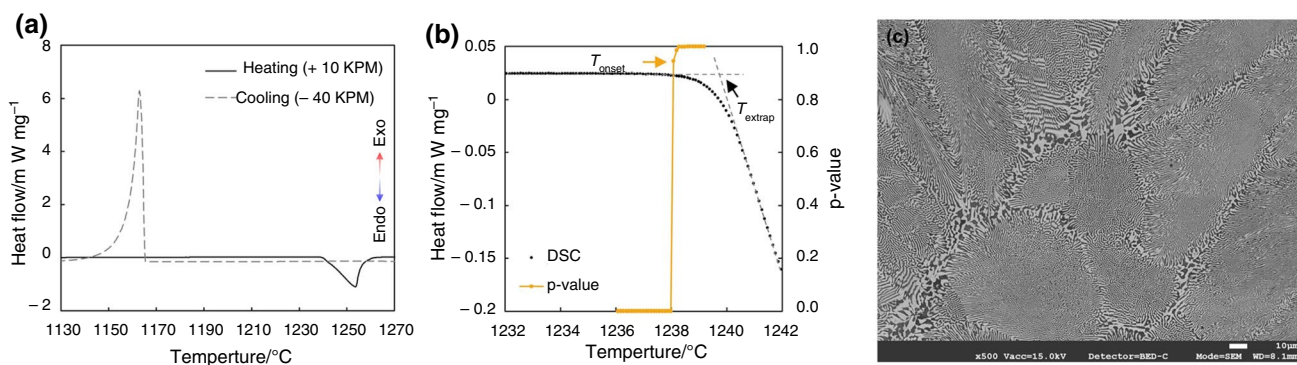


Fig. 8 **a** DSC curves of Co–13Nb alloy during melting and solidification **b** computed p–values, T_{onset} (1238.1 °C), and T_{extrap} (1239.7 °C) **c** solidification microstructure showing regular eutectic lamellae

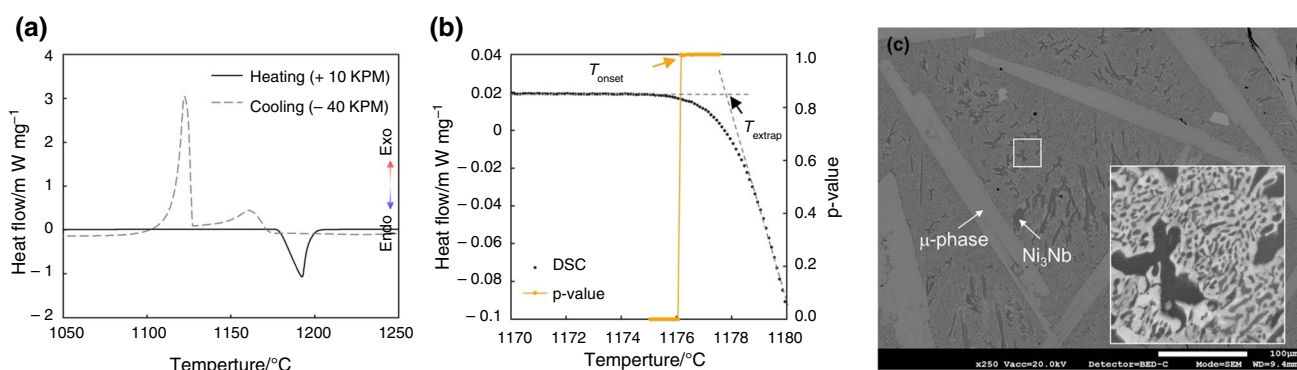


Fig. 9 **a** DSC curves of Ni–41Nb alloy during melting and solidification **b** computed p–values, T_{onset} (1176.2 °C), and T_{extrap} (1178.2 °C) **c** solidification microstructure showing a mixture of faceted μ -phase, small dendritic Ni_3Nb and irregular eutectic structure

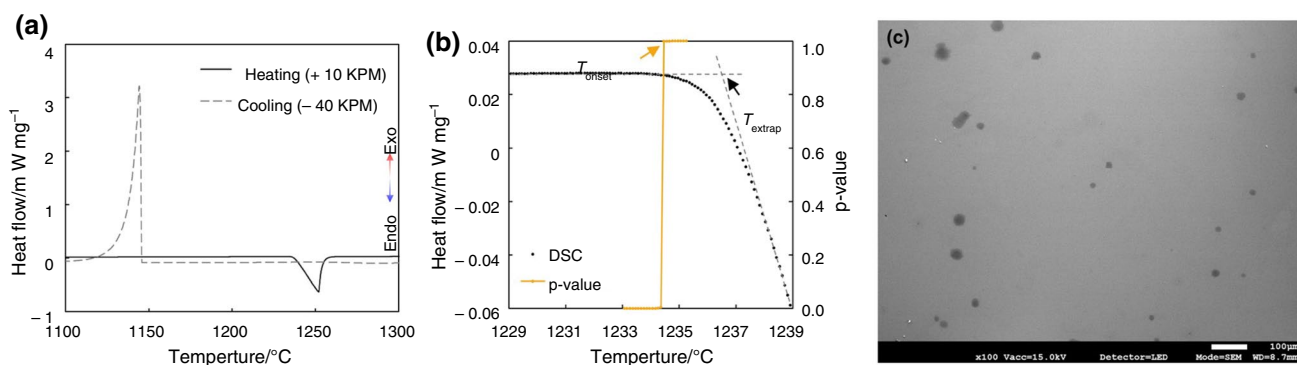


Fig. 10 **a** DSC curves of Ni–45Pd alloy during melting and solidification **b** computed p–values, T_{onset} (1234.5 °C), and T_{extrap} (1237.1 °C) **c** solidification microstructure showing homogeneous FCC phase

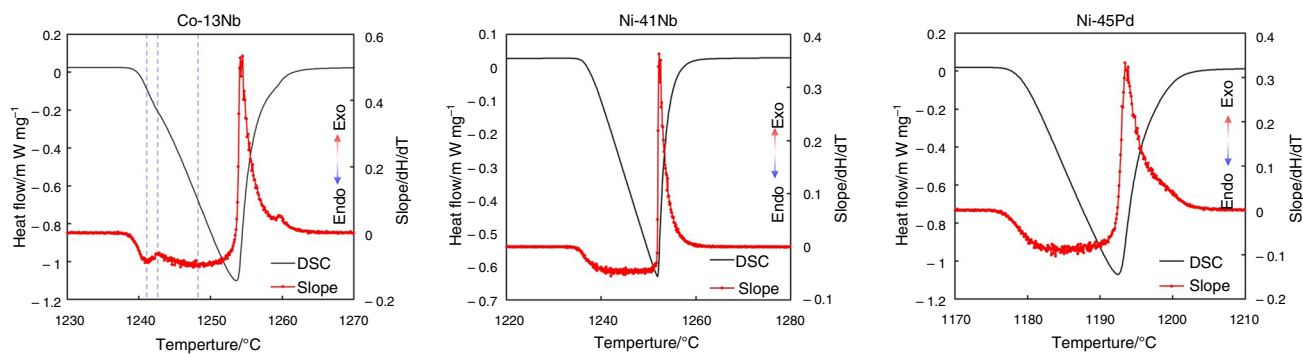


Fig. 11 Slope change of the heat absorption peaks. Co–13Nb alloy encounters two inflections of the slope during melting marked with dashed lines

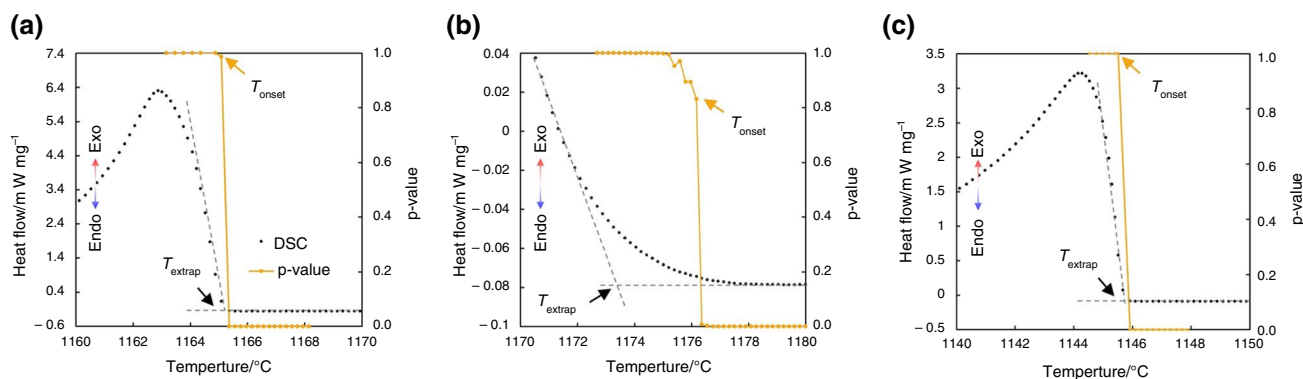


Fig. 12 Computed p -values during solidification of **a** Co–13Nb **b** Ni–41Nb **c** Ni–45Pd alloys

departure of the solidification signal from the baseline is very sharp in eutectic (Co–13Nb) and congruent solidification (Ni–45Pd). T_{onset} and T_{extrap} of Co–13Nb alloy are 1165.1 and 1165.2 °C, respectively, and of Ni–45Pd alloy are 1145.5 and 1145.5 °C, respectively. In the case of Ni–41Nb, which is slightly off-eutectic, the formation of solid μ -phase before the eutectic solidification gives a similar departure signal to the melting. For the solidification of μ -phase, T_{onset} and T_{extrap} are 1176.2 and 1173.4 °C, respectively.

Conclusion

In this study, the ADF test is proposed as a method for determining the onset temperature of melting in binary alloys from DSC. The ADF test, which is a unit root test, distinguishes the stationarity of the DSC data at a specified significance level. The temperature at which the first differences of the baseline of the DSC curve loses stationarity with a 95% significance level (p -value = 0.05) can be assumed to be the value of T_{onset} . Although the determination of T_{extrap} by the extrapolation method is a function

of the sharpness of the reaction kinetics in DSC signal and the choice of the linear portion of the heat absorption peak, the stationarity test depends only on the baseline. The proposed method is validated with a standard reference alloy (Ag–40Cu), wherein the result showed a definite change in p -values at T_{onset} from 0 to 1. The method was also applied to determine the departure temperature of melting and solidification in three binary alloys, Co–13Nb, Ni–41Nb, and Ni–45Pd. The influences from the bluntness of the transition from the baseline to the heat absorption peak and from the inflections in the peak were successfully eliminated.

Supplementary Information The online version contains supplementary material available at <https://doi.org/10.1007/s10973-023-12575-6>.

Acknowledgements This study was supported by the National Research Foundation of Korea (NRF- 2021M3A7C2089767 and 2021M3H4A6A01045764).

Authors' contributions JP, K-WM, C-SO contributed to Conceptualization; JP, K-WM, YL contributed to Methodology; JP, K-WM, J-HK, JJ, DK contributed to Formal analysis and investigation; JP contributed to Writing – original draft preparation; JP, K-WM, C-SO, JHK, JJ, YL, DK contributed to Writing – review and editing.

Declarations

Conflict of interests The authors declare that they have no conflict of interest.

References

1. ASTM. Standard test method for melting and crystallization temperatures by thermal analysis. USA: ASTM International; 2018.
2. ASTM. Standard test method for temperature calibration of differential scanning calorimetry and differential thermal analyzers. USA: ASTM International; 2018.
3. Boettinger WJ, Kattner UR, Moon KW, Perepezko JH. DTA and Heat-flux DSC measurements of alloy melting and freezing, special publication 960–15. Washington DC: U.S. Department of Commerce; 2006.
4. Bedford RE, Bonnier G, Maas H, Pavese F. Recommended values of temperature on the international temperature scale of 1990 for a selected set of secondary reference points. *Metrologia*. 1996;33:133–54. <https://doi.org/10.1088/0026-1394/33/2/3>.
5. Dickey DA. Stationarity Issues in Time Series Models. *Proc SAS Users Group Int*. 2010;30:192–230.
6. Dickey DA, Fuller WA. Distribution of the Estimators for Autoregressive Time Series with a Unit Root. *J Am Stat Assoc*. 1979;74:427–31. <https://doi.org/10.1080/01621459.1979.10482531>.
7. Van Rossum G, Drake FL. *Python 3 Reference Manual*. Scotts Valley: CreateSpace; 2009.
8. Seabold S, Perktold J. Statsmodels econometric and statistical modeling with python. *Proc Python Sci Conf*. 2010. <https://doi.org/10.25080/Majora-92bf1922-011>.
9. Subramanian PR, Perepezko JH. The Ag-Cu (Silver-Copper) system. *J Phase Equilib*. 1993;14:62–75. <https://doi.org/10.1007/BF02652162>.
10. Stein F, Jiang D, Palm M, Sauthoff G, Gruner D, Kreiner G. Experimental reinvestigation of the Co–Nb phase diagram. *Intermetallics*. 2008;16:785–92. <https://doi.org/10.1016/j.intermet.2008.02.017>.
11. Duerden IJ, Hume-Rothery W. The equilibrium diagram of the system niobium-nickel. *J Less-Common Met*. 1966;11:381–438. [https://doi.org/10.1016/0022-5088\(66\)90083-X](https://doi.org/10.1016/0022-5088(66)90083-X).
12. Nash A, Nash P. The Ni-Pd (Nickel-Palladium) system. *Bull Alloy Phase Diagrams*. 1984;5:446–50. <https://doi.org/10.1007/BF02872890>.

Publisher's Note Springer Nature remains neutral with regard to jurisdictional claims in published maps and institutional affiliations.

Springer Nature or its licensor (e.g. a society or other partner) holds exclusive rights to this article under a publishing agreement with the author(s) or other rightsholder(s); author self-archiving of the accepted manuscript version of this article is solely governed by the terms of such publishing agreement and applicable law.